JOURNAL OF SOLID STATE CHEMISTRY 11, 301–313 (1974)

Structural Aspects of the Metal–Insulator Transition in V_5O_9

M. MAREZIO*

Laboratoire des Rayons X, CNRS, B.P. No. 166, Centre de Tri, 38042 Grenoble CEDEX, France

AND

P. D. DERNIER AND D. B. McWHAN†

Bell Laboratories, Murray Hill, New Jersey 07974

AND

S. KACHI

Department of Chemistry, Faculty of Science, Kyoto University, Kyoto, Japan

Received December 5, 1973

V_5O_9, a member of the homologous series V_nO_{2n-1}, undergoes a metal–insulator transition with decreasing temperature at ~135°K. The structures of both phases have been refined at 298 and 110°K from single-crystal data. The triclinic structures ($P\bar{1}$) consists of layers of VO_6 octahedra extending indefinitely in the a–b plane and truncated by a shear plane after every 5 octahedra along the c axis. The average V–O distances for the V atoms at 298°K are for independent atoms 1–6: 1.949, 1.959, 1.965, 1.973, 1.967, and 1.971 Å, respectively. At 110°K the distances are 1.929, 1.975, 1.954, 1.994, 1.954, and 1.986 Å. These values are interpreted as evidence for charge localization in the insulating phase with alternate strings of V^{4+} ions and predominantly V^{3+} ions running along the pseudorutile c axis (3^+ chain is atoms 6–4–2–4–6 and 4^+-chain is 5–3–1–3–5). The oxygen atoms in the insulating phase relax toward V^{4+} string in the a_R and b_R directions and away from the V^{3+} string. The shear planes allow the vanadium atoms to move along the c_R axis so as to compensate for the change in length of alternate chains. Short V–V distances comparable to those in VO_2 are not observed; however, the structure has multiple possible patterns of metal–metal bonds due to edge sharing of octahedra both along the pseudorutile c axis and between adjacent chains at the shear planes.

Introduction

Metal–insulator transitions occur as a function of temperature in many oxides of titanium and vanadium. In the Magneli phases between the sesquioxide, M_2O_3, and the dioxide, MO_2, there is the possibility of transitions which involve charge localization into covalent bonds. In the metallic phase all the transition metal atoms have an average charge, but at lower temperatures the electrons could be thought of as localizing into distinct 3^+ and 4^+ sites. This is similar in concept to the original model by Verwey *et al.* (*1*) for Fe_3O_4. These oxides occur as ordered phases of the composition M_nO_{2n-1}, with $n = 3, 4, 5, \ldots$ (i.e., $M_2O_3 + (n-2)MO_2$). The structures are related to that of rutile, TiO_2, in that they consist of rutilelike blocks which are infinite in two dimensions and n MO_6 octahedra wide in the third (*2*). These blocks are connected by octahedra which share faces

* Part of this work done while at Bell Laboratories, Murray Hill, NJ.

† Part of this work done while at Laboratoire de Magnetisme, CNRS, B.P. No. 166, Centre de Tri, 38042 Grenoble Cedex, France.

along the $1\bar{2}1$ plane of rutile. At the metal–insulator transitions there are discontinuous changes in many physical properties with, for example, increases in the resistivity and decreases in the magnetic susceptibility (*3*). Also, more microscopic measurements such as the ^{51}V nuclear magnetic resonance show changes at the transition from sites of magnetic character to some sites of nonmagnetic character with decreasing temperature (*4*). This is usually interpreted in terms of a transition in which the electrons have localized into a covalent bond between 2 transition metal atoms so that the final spin state is a singlet. Accurate determinations of the crystal structures of these oxides above and below the transitions provide a test of these concepts. There are $2n$ metal sites in the crystallographic unit cell and one of the simplest materials which has a transition is Ti_4O_7 with four $3d$ electrons to distribute over 8 sites. There are 2 transitions in Ti_4O_7, one at 150°K and a second at 130°K (*5*). The resistivity increases markedly at both transitions, but the large decrease in magnetic susceptibility occurs at the higher transition (*6*). Determinations of the crystal structures have been made at 298, 140, and 120°K by X-ray diffraction methods (*7*). Above 150°K the Ti sites are quite similar with an average charge on each of 3.5 as determined from the average Ti–O interatomic distance in each TiO_6 octahedron. Below 130°K the electrons were found to localize into alternate chains of 3^+ and 4^+ sites, and adjacent 3^+ sites paired to form metal–metal bonds. In the intermediate phase no evidence was found for charge localization, but anomalously large thermal displacements were observed. In order to rationalize this with the observed electrical and magnetic properties, it was suggested that the charge was localized into pair bonds but that there was no long-range correlation between bonds. In this model the lower transition is viewed as one from a liquid of pair bonds to a state with ordered bonds (*7*). In the analogous phase containing vanadium, i.e., V_4O_7, there are twelve $3d$ electrons to distribute over 8 vanadium sites. A metal–insulator transition occurs at 250°K, and then a paramagnetic–

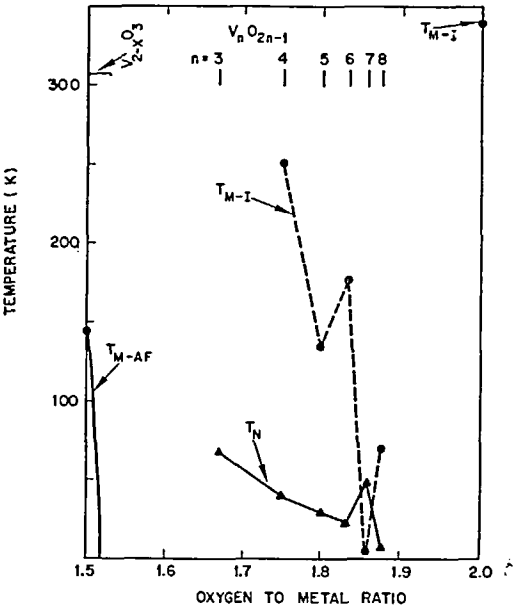

FIG. 1. Transition temperatures vs composition in the system VO_x with $1.5 < x < 2.0$ showing the even–odd relation between the metal–insulator transition temperature in the phases V_nO_{2n-1} and also the decreases toward 0°K of both the M–I and the magnetic transition temperatures with increasing n.

antiferromagnetic transition occurs at 40°K (*3*). The structural studies again show separation of charge into alternate chains of V^{3+} and V^{4+} sites running along the pseudo-rutile c axis (*8*). The V^{3+} sites show some evidence for a pairing, but only 2 of the 4 V^{4+} sites appear to be paired. The nature of the transition in V_4O_7 is also different from that in Ti_4O_7, or from those in higher members of the vanadium series, in that the metal–insulator transition is almost continuous, whereas it is strongly first order in the other materials. The transition temperatures in the vanadium series are plotted vs the oxygen to metal ratio in Fig. 1. With increasing n (decreasing percentage of possible V^{3+} sites) the metal–insulator transition temperatures decrease toward 0°K as do the paramagnetic to antiferromagnetic transition temperatures. However, the former do not decrease smoothly but exhibit an even–odd relation with the members with n even having a higher transition temperature relative to neighboring members

with n odd (*3*). It is therefore of interest to extend the crystallographic studies to an odd member of the series, and this paper reports the determination of the crystal structure of V_5O_9 at 298 and 110°K. The results are compared with the structures of Ti_4O_7 and V_4O_7. It is found that, although there is still charge separation into alternate chains, the pairing probably has to be considered in terms of the different possible pairing configurations allowed by the structure. A description of structure of the Magneli phases is presented which emphasizes the possibility of forming bonds between chains in addition to bonds along the chains.

Experimental

Powder samples of V_5O_9 were made by the usual ceramic techniques. The appropriate mixture of V_2O_3 and V_2O_5 was heated in an evacuated quartz tube at 600°C for 3 days and then at 1000°C for 7 days. Single crystals were then grown from the powder sample by the vapor transport method using $TeCl_4$ (*3*).

Lattice parameters as a function of temperature were determined from X-ray powder diffraction data obtained from a Phillips–Norelco diffractometer fitted with an Air-Products and Chemicals Cryotip device. Copper radiation was used along with silicon powder as internal standard. The Bragg angles of 20 well-resolved reflections were obtained for each temperature, and used as input to a least-squares refinement program. The final parameters are plotted vs temperature in Fig. 2. The values used for structural refinement and interatomic distances are as follows.

298°K	110°K
$a = 5.472$ (1) Å	5.467 (1) Å
$b = 7.003$ (1) Å	7.007 (1) Å
$c = 8.727$ (1) Å	8.735 (1) Å
$\alpha = 97.49°$	97.40°
$\beta = 112.40°$	112.31°
$\gamma = 109.01°$	109.11°

It should be noted that in keeping with previous structural descriptions of Ti_4O_7 and V_4O_7 the unit cell chosen is that of Anderson and Jahnberg, which is left handed (the cell in Ref. (*9*) is right handed). More recently, Horiuchi *et al.* have reported primitive cells for each of the members of the homologous series V_nO_{2n-1} (*10*). The 2 different V_5O_9 unit cells are related by the matrix (*2, 10*)

$$\begin{pmatrix} a \\ b \\ c \end{pmatrix} = \begin{pmatrix} 1 & 0 & 0 \\ 0 & 1 & 0 \\ 2 & 3 & \bar{1} \end{pmatrix} \begin{pmatrix} a \\ b \\ c \end{pmatrix}.$$

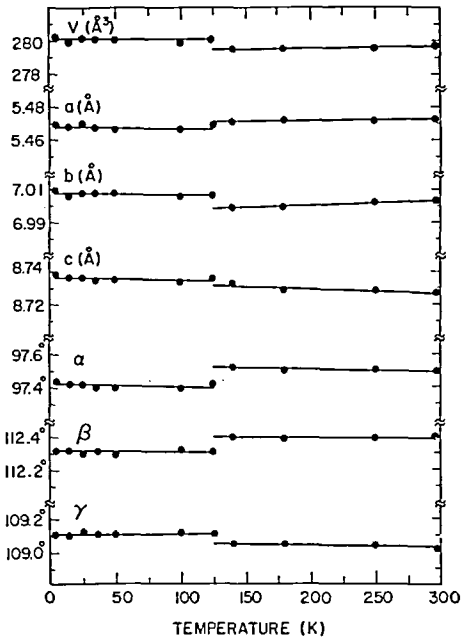

FIG. 2. Lattice parameters and unit cell volume vs temperature for V_5O_9.

Single-crystal intensity measurements were taken with a paper-tape-controlled automatic GE XRD-5 diffractometer. Single Zr-filtered molybdenum radiation was used with an 8° take-off angle, scintillation counter, and decade scalar. Integrated intensities were obtained by the stationary crystal–stationary counter technique. A spherical specimen of radius $R = 0.012$ cm was ground from a portion of a needle-shaped crystal of V_5O_9. This sphere was oriented with the $[20\bar{2}]$ zone axis parallel with the Φ circle axis of the diffractometer. At 298°K all reflections in the

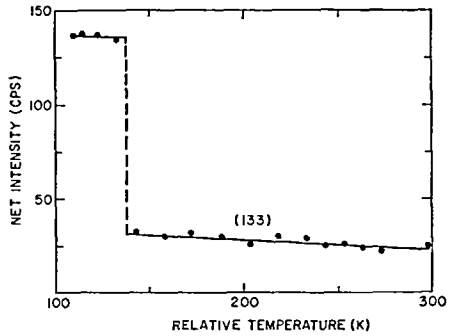

FIG. 3. Net intensity of the reflection (133) vs relative temperature for a sphere of V_5O_9 showing the strong first-order nature of the transition.

upper hemisphere within a 2θ range of 30–70° were measured with the diffractometer in fully automatic mode. Intensity scalars were collected on each peak maximum and ±2° off the peak. In order to check sample orientation and beam stability a standard reflection (030) was measured after every 60 reflections. The total number of reflections measured were 1501, of which 1457 were well above background.

At 110°K the procedure and equipment for collecting data were identical to those used for V_4O_7 (*8*). Only reflections well above background at 298°K were measured at low temperature. In Fig. 3 the intensity of the reflection (133) is plotted vs a relative temperature scale. The sharp increase in intensity at ~135°K was a sensitive indicator of phase change, and therefore this reflection was used as a low-temperature standard. Also, the (030) was used as a second standard in order to check the sample orientation and the buildup of ice. The total number of observed independent reflections at 110°K was 782. The Lorentz, polarization, and spherical absorption programs were applied in order to convert the net intensity data into structure factors. The linear absorption coefficient for V_5O_9 with MoKα radiation was 85.6 cm^{-1}, yielding a $\mu R = 1.04$. The intensities of all Friedel pairs of weak reflections in the equatorial zone were measured by hand at

TABLE I

POSITIONAL PARAMETERS

	298°K	110°K		298°K	110°K
V(1) x	0.0	0.0	z	0.0791 (3)	0.0809 (2)
y	0.5	0.5	O(3) x	0.3942 (4)	0.3941 (5)
z	0.0	0.0	y	0.5340 (3)	0.5345 (3)
V(2) x	0.0	0.0	z	0.1369 (3)	0.1379 (3)
y	0.0	0.0	O(4) x	0.9170 (4)	0.9217 (5)
z	0.0	0.0	y	0.4892 (3)	0.4893 (4)
V(3) x	0.54953 (9)	0.54899 (15)	z	0.1994 (3)	0.1937 (3)
y	0.83654 (7)	0.83275 (9)	O(5) x	0.2138 (4)	0.2164 (5)
z	0.20294 (6)	0.19766 (7)	y	0.1883 (3)	0.1901 (3)
V(4) x	0.55815 (9)	0.57287 (14)	z	0.2408 (3)	0.2449 (2)
y	0.34500 (7)	0.35132 (9)	O(6) x	0.7283 (4)	0.7287 (5)
z	0.20808 (6)	0.21398 (6)	y	0.1503 (3)	0.1479 (3)
V(5) x	0.13748 (9)	0.13267 (13)	z	0.3222 (3)	0.3220 (2)
y	0.17333 (7)	0.17133 (9)	O(7) x	0.9490 (4)	0.9483 (5)
z	0.42045 (6)	0.41555 (6)	y	0.8650 (3)	0.8653 (3)
V(6) x	0.14709 (9)	0.14989 (13)	z	0.3664 (2)	0.3674 (2)
y	0.67629 (7)	0.67757 (8)	O(8) x	0.4815 (4)	0.4887 (5)
z	0.42466 (6)	0.42581 (6)	y	0.7995 (3)	0.8014 (3)
O(1) x	0.6475 (4)	0.6490 (5)	z	0.4184 (3)	0.4175 (3)
y	0.8505 (3)	0.8517 (3)	O(9) x	0.7708 (4)	0.7757 (5)
z	0.0230 (2)	0.0265 (2)	y	0.5334 (3)	0.5379 (3)
O(2) x	0.1647 (4)	0.1671 (5)	z	0.4596 (2)	0.4624 (2)
y	0.8064 (3)	0.8067 (3)			

TABLE II

THERMAL PARAMETERS ($\times 10^4$)

	298°K	110°K		298°K	110°K
V(1)	β_{11} 54 (2)	53 (3)		β_{12} 26 (4)	13 (5)
	β_{22} 25 (1)	25 (2)		β_{13} 19 (3)	18 (4)
	β_{35} 21 (1)	16 (1)		β_{23} 8 (2)	6 (2)
	β_{12} 18 (1)	23 (2)	O(3)	β_{11} 57 (6)	31 (8)
	β_{13} 14 (1)	17 (1)		β_{22} 30 (3)	38 (4)
	β_{23} 2 (1)	8 (1)		β_{33} 24 (2)	27 (2)
V(2)	β_{11} 67 (2)	38 (3)		β_{12} 20 (4)	12 (5)
	β_{22} 36 (1)	29 (2)		β_{13} 14 (3)	16 (4)
	β_{33} 24 (1)	19 (1)		β_{23} 5 (2)	21 (2)
	β_{12} 27 (1)	19 (2)	O(4)	β_{11} 47 (6)	41 (8)
	β_{13} 22 (1)	2 (1)		β_{22} 36 (4)	31 (4)
	β_{23} 8 (1)	−5 (1)		β_{33} 23 (2)	29 (2)
V(3)	β_{11} 51 (2)	77 (2)		β_{12} 11 (4)	13 (5)
	β_{22} 26 (1)	37 (1)		β_{13} 18 (3)	27 (4)
	β_{33} 21 (1)	11 (1)		β_{23} 3 (2)	13 (2)
	β_{12} 16 (1)	41 (2)	O(5)	β_{11} 68 (7)	31 (7)
	β_{13} 12 (1)	0 (1)		β_{22} 38 (4)	33 (4)
	β_{23} 3 (1)	−1 (1)		β_{33} 19 (2)	13 (2)
V(4)	β_{11} 55 (2)	35 (2)		β_{12} 20 (4)	9 (5)
	β_{22} 28 (1)	29 (1)		β_{13} 18 (3)	14 (3)
	β_{33} 18 (1)	12 (1)		β_{23} 9 (2)	5 (2)
	β_{12} 20 (1)	8 (1)	O(6)	β_{11} 43 (6)	54 (8)
	β_{13} 16 (1)	8 (1)		β_{22} 29 (3)	19 (3)
	β_{23} 3 (1)	8 (1)		β_{33} 19 (2)	11 (2)
V(5)	β_{11} 53 (2)	46 (2)		β_{12} 16 (4)	18 (5)
	β_{22} 25 (1)	20 (1)		β_{13} 12 (3)	12 (3)
	β_{33} 20 (1)	17 (1)		β_{23} 3 (2)	4 (2)
	β_{12} 15 (1)	14 (1)	O(7)	β_{11} 53 (6)	38 (8)
	β_{13} 21 (1)	20 (1)		β_{22} 21 (3)	25 (4)
	β_{23} 2 (1)	7 (1)		β_{33} 21 (2)	15 (2)
V(6)	β_{11} 56 (2)	69 (2)		β_{12} 16 (4)	12 (5)
	β_{22} 31 (1)	29 (1)		β_{13} 16 (3)	12 (3)
	β_{33} 21 (1)	14 (1)		β_{23} 2 (2)	6 (2)
	β_{12} 23 (1)	29 (1)	O(8)	β_{11} 51 (6)	26 (8)
	β_{13} 21 (1)	22 (1)		β_{22} 42 (4)	23 (4)
	β_{23} 7 (1)	11 (1)		β_{33} 27 (3)	30 (2)
O(1)	β_{11} 58 (6)	24 (8)		β_{12} 22 (4)	14 (5)
	β_{22} 29 (4)	27 (4)		β_{13} 18 (3)	9 (4)
	β_{33} 22 (2)	18 (2)		β_{23} 5 (2)	13 (2)
	β_{12} 9 (4)	3 (5)	O(9)	β_{11} 55 (6)	19 (8)
	β_{13} 20 (3)	6 (3)		β_{22} 27 (3)	13 (3)
	β_{23} 2 (2)	6 (2)		β_{33} 16 (2)	14 (2)
O(2)	β_{11} 57 (6)	62 (8)		β_{12} 13 (4)	0 (5)
	β_{22} 34 (4)	21 (4)		β_{13} 15 (3)	10 (3)
	β_{33} 27 (2)	17 (2)		β_{23} 6 (2)	3 (2)

both 298 and 110°K. Within experimental limits no differences in intensities between (hkl) and $(\bar{h}k\bar{l})$ were detected at either temperature, suggesting that the structure remains centric over this range.

Least-squares refinements were carried out by using computer programs written by Prewitt and Busing *et al.* (*11*). The starting positional parameters for the 298°K refinement were those given for Ti_5O_9 reported by Andersson and Jahnberg. All refinements used scattering factors for neutral atoms and the real and imaginary anomalous dispersion coefficients for Mo radiation (*12*). In the first few cycles of refinement the scale factor, secondary extinction coefficients, 39 positional parameters, and 14 isotropic thermal parameters were varied. The conventional R and wR factors were 0.045 and 0.065, respectively. The secondary extinction coefficient converged to 0.4×10^{-4}. Anisotropic thermal parameters were introduced in the final cycles of refinement resulting in new values of $R = 0.034$ and $wR = 0.048$. Starting positional parameters for the 110°K refinement were those for V_5O_9 at 298°K. The R and wR factors using isotropic thermal parameters were 0.045 and 0.072, respectively. The values dropped to 0.021 and 0.031 respectively, upon introduction of anisotropic thermal parameters. No change in secondary extinction coefficient was observed. The final positional and thermal parameters are listed in Tables I and II, respectively. A list of observed and calculated structure factors for both temperatures is omitted, but is available.[1] The interatomic distances and thermal data calculated by the program ORFFE (*13*) are reported in Tables III–VI.

Results and Discussion

Figure 4 shows a projection of the V_5O_9 structure down the triclinic a axis. One can see blocks of a distorted rutile structure which are delineated after every 5 octahedra by crystallographic shear planes. These shear planes run parallel to the triclinic a–b plane so that the rutilelike blocks extend indefinitely in these directions. Along the shear planes the vanadium-occupied octahedra share common edges and faces, whereas inside the rutile

[1] A table of observed and calculated structure factors has been deposited as Document No. NAPS 02363.

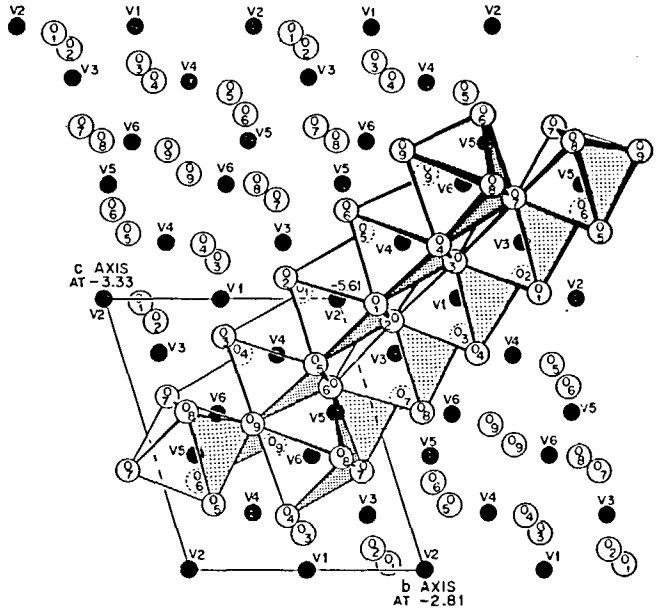

FIG. 4. Projection of the V_5O_9 structure down the triclinic a axis. The b–c plane slopes down and away from the origin. The shaded set of octahedra run roughly parallel to the pseudorutile c axis.

TABLE III

INTERATOMIC DISTANCES (Å) IN V OCTAHEDRA[a]

	298°K	110°K		298°K	110°K
V(1)–O(2) × 2	1.943	1.946	O(1)–O(5)	2.694	2.746
O(3) × 2	1.940	1.940	O(1)–O(6)	2.928	2.961
O(4) × 2	1.963	1.901	O(1)–O(3)	2.786	2.801
average	1.949	1.929	O(9)–O(4)	2.694	2.767
O(2)–O(3) × 2	2.608	2.599	O(9)–O(5)	2.888	2.901
O(2)–O(3) × 2	2.877	2.889	O(9)–O(6)	2.689	2.734
O(2)–O(4) × 2	2.757	2.708	O(4)–O(3)	2.832	2.869
O(2)–O(4) × 2	2.766	2.732	O(4)–O(6)	2.786	2.833
O(3)–O(4) × 2	2.795	2.733	O(5)–O(3)	2.713	2.716
O(3)–O(4) × 2	2.725	2.700	O(5)–O(6)	2.742	2.748
V(2)–O(1) × 2	1.973	1.978	V(5)–O(5)	1.776	1.725
O(2) × 2	1.922	1.932	–O(6)	2.010	1.982
O(5) × 2	1.981	2.061	–O(7)	2.116	2.132
av	1.959	1.975	–O(8)	1.949	1.956
O(1)–O(2) × 2	2.810	2.819	-O(7)	1.965	1.955
O(2)–O(1) × 2	2.697	2.710	–O(9)	1.984	1.976
O(1)–O(5) × 2	2.894	2.900	av	1.967	1.954
O(1)–O(5) × 2	2.694	2.746	O(9)–O(5)	3.006	2.963
O(2)–O(5) × 2	2.785	2.831	O(9)–O(6)	2.648	2.625
O(2)–O(5) × 2	2.734	2.754	O(9)–O(7)	2.575	2.551
V(3)–O(1)	1.847	1.782	O(9)–O(8)	2.788	2.764
–O(2)	1.888	1.876	O(7)–O(5)	2.854	2.847
–O(3)	1.918	1.893	O(7)–O(6)	2.649	2.630
–O(6)	2.024	2.043	O(7)–O(7)	2.549	2.536
–O(7)	2.029	2.036	O(7)–O(8)	2.895	2.869
–O(8)	2.083	2.094	O(7)–O(8)	2.671	2.618
av	1.965	1.954	O(7)–O(6)	2.656	2.650
O(3)–O(1)	2.728	2.718	O(5)–O(8)	2.774	2.754
O(3)–O(2)	2.608	2.599	O(5)–O(6)	2.942	2.923
O(3)–O(7)	2.858	2.858	V(6)–O(4)	1.880	1.929
O(3)–O(8)	2.656	2.638	–O(6)	2.105	2.110
O(6)–O(1)	2.917	2.886	–O(7)	1.967	1.975
O(6)–O(2)	2.942	2.927	–O(8)	1.777	1.805
O(6)–O(7)	2.649	2.630	–O(9)	2.133	2.124
O(6)–O(8)	2.793	2.753	–O(9)	1.962	1.970
O(1)–O(2)	2.795	2.777	av	1.971	1.986
O(1)–O(7)	2.785	2.771	O(4)–O(7)	2.754	2.796
O(8)–O(2)	2.820	2.808	O(4)–O(8)	2.822	2.841
O(8)–O(7)	2.671	2.618	O(4)–O(9)	2.694	2.767
V(4)–O(1)	1.937	2.019	O(4)–O(9)	2.868	2.895
–O(3)	1.872	1.895	O(6)–O(7)	2.656	2.650
–O(4)	1.930	1.923	O(6)–O(8)	2.933	2.974
–O(5)	1.996	2.046	O(6)–O(9)	2.648	2.625
–O(6)	2.048	2.045	O(6)–O(9)	2.689	2.734
–O(9)	2.052	2.035	O(8)–O(7)	2.971	3.009
av	1.973	1.994	O(8)–O(9)	2.854	2.896
O(1)–O(3)	2.761	2.786	O(9)–O(7)	2.575	2.551
O(1)–O(4)	2.899	2.919	O(9)–O(9)	2.551	2.540

[a] The standard deviations for all V–O distances in this Table are ±0.002 Å and ±0.003 Å for all O–O distances.

TABLE IV

V–V DISTANCES (Å)[a]

	298°K	110°K		298°K	110°K
V(1)–V(4)*c* × 2	3.500	3.547	–V(1)*c*	3.532	3.501
–V(4)*c* × 2	3.532	3.501	–V(2)*e*	2.878	2.947
–V(6)*c* × 2	3.434	3.447	–V(6)*e*	2.947	2.891
–V(2)*c* × 2	3.502	3.504	–V(5)*cb*	3.746	3.739
–V(3)*e* × 2	2.823	2.806	–V(6)*eb*	3.039	2.997
V(2)–V(3)*c* × 2	3.493	3.500	V(5)–V(6)*c*	3.501	3.506
–V(3)*c* × 2	3.541	3.507	–V(6)*c*	3.503	3.503
–V(1)*c* × 2	3.502	3.504	–V(3)*e*	2.958	2.950
–V(5)*c* × 2	3.412	3.384	–V(4)*c*	3.494	3.507
–V(4)*e* × 2	2.878	2.947	–V(4)*c*	3.676	3.615
V(3)–V(6)*c*	3.472	3.496	–V(2)*c*	3.412	3.384
–V(6)*c*	3.653	3.604	–V(6)*fb*	2.768	2.783
–V(4)*c*	3.464	3.437	–V(5)*eb*	3.190	3.210
–V(4)*c*	3.540	3.575	–V(6)*cb*	3.343	3.347
–V(4)*c*	3.397	3.385	–V(4)*cb*	3.746	3.739
–V(1)*e*	2.823	2.806	–V(3)*eb*	3.096	3.168
–V(2)*c*	3.493	3.500	V(6)–V(5)*c*	3.501	3.506
–V(2)*c*	3.541	3.507	–V(5)*c*	3.503	3.503
–V(5)*e*	2.958	2.950	–V(5)*fb*	2.768	2.783
–V(6)*cb*	3.777	3.819	–V(5)*cb*	3.343	3.347
–V(5)*eb*	3.096	3.168	–V(3)*c*	3.472	3.496
V(4)–V(3)*c*	3.464	3.437	–V(3)*c*	3.653	3.604
–V(3)*c*	3.540	3.575	–V(3)*cb*	3.777	3.819
–V(3)*c*	3.397	3.385	–V(4)*e*	2.947	2.891
–V(5)*c*	3.494	3.507	–V(4)*eb*	3.039	2.997
–V(5)*c*	3.676	3.615	–V(1)*c*	3.434	3.447
–V(1)*c*	3.500	3.547	–V(6)*eb*	3.208	3.214

[a] The symbols *c*, *e*, and *f* refer to V–V distances across a shared octahedral corner, edge, or face, respectively. The symbol *b* indicates V–V distances between rutile blocks. The standard deviations for all distances in this table are ±0.001 Å.

blocks only edge and corner sharing occurs. One should note that for V_5O_9, as well as the entire homologous series V_nO_{2n-1}, the oxygen array remains essentially hexagonal close-packed. It is only the arrangement of vanadium occupancy which varies across the series.

The structure of V_5O_9 has 6 crystallographically independent vanadium sites. The chains which run along the pseudorutile *c* axis are numbered for clarity in the same way as in V_4O_7 with even and odd numbers referring to different chains. The chains as seen in Fig. 4 are V(5)–V(3)–V(1)–V(3)–V(5) and V(6)–V(4)–V(2)–V(4)–V(6). V_5O_9 is the lowest member of the homologous series which has a vanadium atom whose nearest-neighbor vanadium atom coordination is entirely rutilelike with only 2 shared octahedral edges and all other contacts being through corner oxygens. These atoms are V(1) and V(2) at the center of each chain, and they occupy special positions, being at a center of symmetry. In V_4O_7 it was found that the average V–O distance in each VO_6 octahedra changed markedly at the metal–insulator transition, and a similar effect is observed in V_5O_9. The approximate electro-

TABLE V

ROOT MEAN-SQUARE VALUES (Å)

	298°K	110°K		298°K	110°K
V(1) r_1	0.063 (2)	0.057 (3)	r_3	0.091 (4)	0.083 (5)
r_2	0.076 (2)	0.062 (2)	O(3) r_1	0.073 (5)	0.049 (8)
r_3	0.087 (2)	0.079 (2)	r_2	0.079 (4)	0.066 (6)
V(2) r_1	0.068 (2)	0.057 (3)	r_3	0.090 (4)	0.107 (4)
r_2	0.086 (2)	0.060 (2)	O(4) r_1	0.065 (5)	0.046 (8)
r_3	0.090 (2)	0.106 (2)	r_2	0.077 (4)	0.080 (6)
V(3) r_1	0.069 (2)	0.054 (2)	r_3	0.097 (4)	0.095 (4)
r_2	0.074 (1)	0.056 (2)	O(5) r_1	0.073 (5)	0.043 (8)
r_3	0.088 (1)	0.117 (1)	r_2	0.085 (4)	0.066 (5)
V(4) r_1	0.059 (2)	0.057 (2)	r_3	0.088 (4)	0.087 (5)
r_2	0.078 (1)	0.061 (2)	O(6) r_1	0.064 (5)	0.054 (7)
r_3	0.084 (1)	0.084 (2)	r_2	0.071 (5)	0.058 (6)
V(5) r_1	0.054 (2)	0.054 (2)	r_3	0.084 (4)	0.078 (6)
r_2	0.074 (1)	0.062 (2)	O(7) r_1	0.057 (6)	0.062 (6)
r_3	0.088 (1)	0.078 (1)	r_2	0.075 (4)	0.067 (5)
V(6) r_1	0.059 (2)	0.052 (2)	r_3	0.085 (4)	0.071 (6)
r_2	0.080 (1)	0.061 (2)	O(8) r_1	0.068 (5)	0.046 (9)
r_3	0.083 (1)	0.089 (1)	r_2	0.087 (4)	0.063 (6)
O(1) r_1	0.071 (5)	0.049 (9)	r_3	0.100 (4)	0.104 (4)
r_2	0.073 (5)	0.075 (5)	O(9) r_1	0.067 (5)	0.035 (12)
r_3	0.095 (4)	0.084 (6)	r_2	0.074 (5)	0.061 (7)
O(2) r_1	0.065 (6)	0.065 (6)	r_3	0.080 (5)	0.068 (6)
r_2	0.086 (4)	0.069 (6)			

static charges can be calculated from a plot of bond strength versus bond length as discussed in Ref. (*8*), bond strength = 226 exp [−3.0348 (bond length)]. The values calculated for the different vanadium atoms at 298 and 110°K, respectively, are

$V(2) = 3.7 \rightarrow 3.5$ $V(1) = 3.8 \rightarrow 4.1$
$V(4) = 3.5 \rightarrow 3.2$ $V(3) = 3.6 \rightarrow 3.8$
$V(6) = 3.5 \rightarrow 3.3$ $V(5) = 3.6 \rightarrow 3.8$

If the charge is uniformly distributed, then V_5O_9 is formally $V_2O_3 + 3VO_2$ and the average charge is 3.6. At 298°K the average of all the vanadium charges is 3.6, but as with V_4O_7 at room temperature there are individual deviations from the average. The atoms which have the greatest similarity with rutile have a slightly larger charge (V(1) and V(2)). At the transition there is a clear decrease in charge of .0.2–0.3 for each vanadium in the 6–4–2–4–6 chain and a similar increase in charge for each vanadium in the 5–3–1–3–5 chain. If the charge was localized as much as possible, then one chain would have an average charge of 3.2 and the other 4.0, which is in reasonable agreement with the observed values of 3.3 and 3.9. There are clearly variations depending on the local environment, and such an analysis of local charges from bond lengths cannot be carried too far. However, the experimental evidence clearly favors the separation of charge as much as possible into alternate strings running along the pseudorutile *c* axis as was found in Ti_4O_7 and V_4O_7.

The interpretation of the displacements of the different vanadium and oxygen atoms at the transition is less straightforward because of both the complexity of the structure and the correlations which must exist between the displacements of neighboring atoms. In the case of Ti_4O_7, the Ti^{3+} sites move toward each other so that the Ti–Ti distance between pairs decreases of the order of 0.20 Å. Similarly,

TABLE VI

	298°K	110°K
RMS Components along the Pseudorutile *c* Axis		
V(2)–V(4)	0.090 (2)	0.067 (2)
–V(4)	0.090 (2)	0.067 (2)
V(4)–V(2)	0.078 (1)	0.064 (2)
–V(6)	0.078 (1)	0.063 (2)
V(6)–V(4)	0.082 (1)	0.089 (1)
V(1)–V(3)	0.076 (2)	0.079 (2)
–V(3)	0.076 (2)	0.079 (2)
V(3)–V(1)	0.074 (1)	0.094 (1)
–V(5)	0.074 (1)	0.092 (1)
V(5)–V(3)	0.075 (1)	0.072 (2)
RMS Components along V–V Vectors between Cation Chains		
V(4)–V(5)	0.076 (1)	0.061 (2)
V(5)–V(4)	0.067 (1)	0.054 (2)
V(2)–V(3)	0.082 (2)	0.090 (2)
V(3)–V(2)	0.084 (1)	0.075 (1)
V(4)–V(1)	0.075 (2)	0.060 (2)
V(1)–V(4)	0.083 (2)	0.063 (2)
V(3)–V(6)	0.085 (1)	0.109 (1)
V(6)–V(3)	0.069 (2)	0.061 (2)
RMS Components in the Direction of the V(5)–V(6) Vector		
V(5)–V(6)	0.055 (2)	0.056 (2)
V(6)–V(5)	0.059 (2)	0.058 (2)

in the case of pure VO_2 there is pairing with a decrease in the V–V distance of 0.23 Å (*14*). In terms of the logarithmic relation between bond length and bond order suggested by Pauling [$r_1 - r_2 = 0.33 \ln (n_1/n_2)$, where r is the bond length and n the bond order, and the 0.33 is from the empirical relation above (*15*)] these changes imply a doubling of the bond order in the insulating phase over that in the metallic phase. However, in the vanadium series of Magneli phases there are mixtures of V^{3+} ions with two 3*d* electrons and V^{4+} ions with one 3*d* electron. If two 3*d* electrons from each of adjacent V^{3+} sites were to be involved in forming a bond, then one might expect to observe an even larger change in bond strength and therefore in bond length. In the case of V_4O_7 the 4 V^{3+} sites in the chain do show evidence for the formation of 2 short bonds, but the maximum change in bond length at the transition is only 0.07 Å. A similar change of 0.07 is observed between 2 of the V^{4+} sites in V_4O_7. In V_4O_7 there is evidence from measurement of the variation with temperature of the electrical resistivity (*3*), magnetic susceptibility (*3*), ^{51}V nuclear magnetic resonance (*4*), and structure (*8*) that the transition is only slightly first order and that the amount of pairing increases with decreasing temperature in the insulating phase. The structure of V_4O_7 was refined at a temperature only 50° below the metal–insulator transition so that it was felt that larger changes in bond length would be observed at lower temperatures. However, in V_5O_9 the transition is strongly first order and no changes in metal–metal distances at the transition were observed which exceed 0.06 Å (see Table IV). The NMR results clearly show the existence of some singlet metal–metal bonds (*4*), but the crystallographic data do not show unambiguously the bonding pattern.

In order to try to obtain a unified picture of the metal–insulator transitions in the Magneli phases, an idealized description of the structures is given which is derived from the rutile structure. In all these structures the oxygen network is a distorted hexagonal close-packed array. In rutile half of the octahedral holes of the hexagonal close-packed oxygen array are filled and the other half are empty so one can think of the structure as containing two sublattices of octahedral sites. One consists of the positions 0, 0, 0 and $\frac{1}{2}, \frac{1}{2}, \frac{1}{2}$ and the second consists of $\frac{1}{2}$, 0, 0; 0, $\frac{1}{2}$, $\frac{1}{2}$. In the Magneli phases there are blocks in which one sublattice is occupied and adjacent blocks in which the second sublattice is occupied. The plane between blocks is the $1\bar{2}1$ of rutile. The idealized structure of V_nO_{2n-1} can be thought of as chains of edge-sharing octahedra along the c_R axis, which are n octahedra long and are connected to adjacent chains either by face sharing in the a_R direction or edge sharing in the b_R direction. The basic

unit can be given by $2n$ vanadium octahedra centered at

$$\left(-\frac{\mathbf{a_R}}{4}-(n-1)\,c_R\right),\ldots,\left(-\frac{\mathbf{a_R}}{4}-2\mathbf{c_R}\right),$$
$$\left(-\frac{\mathbf{a_R}}{4}-\mathbf{c_R}\right),\left(-\frac{\mathbf{a_R}}{4}\right),\left(+\frac{\mathbf{a_R}}{4}\right),$$
$$\left(+\frac{\mathbf{a_R}}{4}+c_R\right),\left(+\frac{\mathbf{a_R}}{4}+2\mathbf{c_R}\right),\ldots,$$
$$\left(+\frac{\mathbf{a_R}}{4}+(n-1)\,\mathbf{c_R}\right).$$

The 3-dimensional lattice of vanadium atom positions is then generated by adding to each atom in the basic unit a translation vector of the form

$$\mathbf{T}=m_1\,\mathbf{a_R}+m_2\frac{\mathbf{b_R}}{2}+\left[2(n-1)\,m_1+\left(\frac{n+1}{2}\right)m_2+(2n-1)\,m_3\right]\mathbf{c_R},$$

where n is in V_nO_{2n-1} and m_1, m_2, and m_3 can take values of 0, ±1, ±2, ... In the triclinic unit cells of the different structures there are centers of symmetry at the center of each chain of n octahedra so that, for example, the atoms at $-\mathbf{a_R}/4$ and $(-\mathbf{a_R}/4-(n-1)\mathbf{c_R})$ are crystallographically equivalent (similarly with the pair $(+\mathbf{a_R}/4)$ and $(\mathbf{a_R}/4+(n-1)c_R)$. For members of the series with n odd there will be vanadium atoms in special positions at the center of symmetry. In the idealized structure the chains at $+\mathbf{a_R}/4$ and $-\mathbf{a_R}/4$ are equivalent, but they are inequivalent in the triclinic cell. By considering this simple description of edge- and face-sharing contacts between V atoms, some of the observed properties of the Magneli phases can be rationalized and the importance of edgesharing between rutilelike blocks, in addition to sharing within blocks, is emphasized. In Fig. 5 the chains for V_4O_7 and V_5O_9 are compared both in the a_Rc_R and b_Rc_R planes. Each chain extends indefinitely up and down in the figure. The chains in the top part of the figure represent the basic unit with $m_1=m_2=m_3=0$. Links defined by $m_1=\pm1,\pm2,\ldots$ extend the chain in the a_Rc_R plane. In the lower part of the figure, chains representing the top and the bottom half of the basic unit in the b_Rc_R plane are shown and extend indefinitely as $m_2=\pm1,\pm2,\ldots$. These chains are stacked in the a_R direction so as to have alternate ends of each link sharing faces with the link above or below as shown in the top of Fig. 5. This defines a block which is infinite in two directions and finite in the third. Different blocks are numbered by different values of m_3 and are only joined by corner-sharing contacts.

In Fig. 5, the numbers next to the points give the crystallographic number of the atoms in the triclinic unit cell and the difference between the charge calculated from the V–O distances at room temperature and low temperature. The displacement of the atoms within the unit cell at the transition (i.e., position in insulating phase at low temperature minus the position in the metallic phase at room temperature) is also shown by vectors which have been magnified by a factor of 20. Chains of both the even- and odd-numbered atoms are shown, i.e., sections at $+\mathbf{a_R}/4$ and at $-\mathbf{a_R}/4$ in the notation above or at $x=0$ and $\frac{1}{2}$ along a_R in the conventional rutile cell. It is clear that below the transition there are alternating chains of 3^+ and 4^+ sites as described above. One rationalization for the separation of charge into strings is that it is possible to compensate for the expansion and contraction of octahedra on a local basis, a compensation which is probably favorable from the point of view of minimizing the total elastic energy. Looking down the rutile c axis, the oxygen atoms relax either toward or away from the vanadium at the center of the cell making, it either 4^+ or 3^+, respectively. Because of the crystallographic shear planes the difference in the length of alternate chains of 4^+ and 3^+ octahedra are compensated. It is clear in Fig. 5 that the displacements in V_5O_9 along c_R are such as to contract the 4^+ chain and to expand the 3^+ chain as required by the sizes of the ions. Given the separation of charge, there is no evidence for bonding between chains of different charge at the transition. The vanadium–vanadium distance increases across the shared octahedral faces by ~0.01 Å at the transition, and this distance is still 0.07 Å larger than across the shared face in the corundum structure of V_2O_3 (2.697 Å).

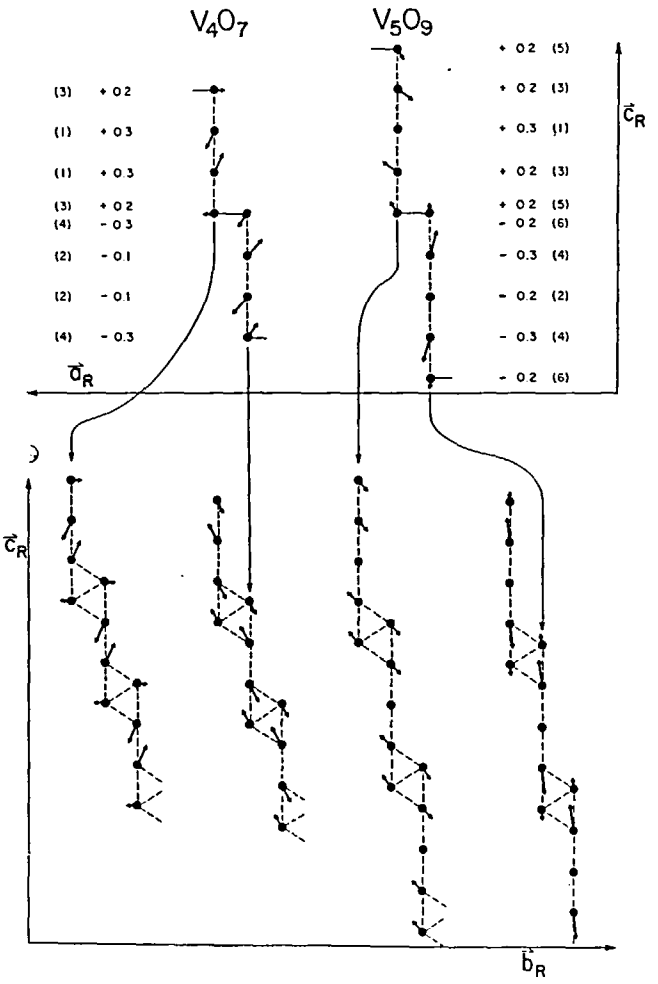

FIG. 5. Idealized projections of the vanadium atoms in V_4O_7 and V_5O_9 in the rutile cell. The charge on the vanadium atoms below the metal–insulator transition minus the charge at room temperature as calculated from the V–O distances are shown along with the number of the atom in parentheses. The displacements of the atoms at low temperature from their positions at room temperature are also shown. The displacements are magnified 20× for clarity and the change in lattice parameters has been neglected. The dashed lines show the edge-sharing contacts where metal–metal bonds might occur. The solid lines are the metal–metal contacts across the shared face of the oxygen octahedra. At the shear planes there are several possible bonding patterns.

Within an infinite chain in the b_Rc_R plane there are possible metal–metal bonds not only along c_R in any one section of the chain but also between sections as can be seen in Fig. 5. It is possible to conceive of forming both single and double bonds by overlap of d orbitals of adjacent vanadium atoms. A priori, there is no obvious reason to expect one particular bonding pattern to predominate over the others. The absence of any V–V distances in insulating V_5O_9 that are comparable to those in insulating VO_2 might be rationalized by assuming that in any macroscopic crystal of V_5O_9 an average of many different bonding patterns are observed by classical X-ray diffraction

methods. The present study on an odd member of the series V_5O_9 gives evidence for the localization of charge along the pseudorutile *c* axis which is similar to that observed in the even members of the series V_4O_7 and Ti_4O_7. However, the exact nature and location of the metal–metal bonds in V_4O_7 and V_5O_9 is not understood at this time.

Acknowledgments

We thank T. M. Rice for many helpful discussions.

References

1. E. J. Verwey, P. W. Haayman, and F. C. Romeijn, *J. Chem. Phys.* **15**, 181 (1947).
2. S. Andersson and L. Jahnberg, *Ark. Kem.* **21**, 413 (1963).
3. S. Kachi, AIP Conf. Proc. No. **10**, 714 (1972).
4. A. C. Gossard, J. P. Remeika, T. M. Rice, H. Yasuoka, K. Kosuge, and S. Kachi *Phys. Rev.* **B9**, 1230 (1974).
5. R. F. Bartholomew and D. F. Frankl, *Phys. Rev.* **187**, 838 (1969).
6. L. N. Mulay and W. J. Danley, *J. Appl. Phys.* **41**, 847 (1970).
7. M. Marezio, D. B. McWhan, P. D. Dernier, and J. P. Remeika, *J. Solid State Chem.* **6**, 213 (1973).
8. M. Marezio, D. B. McWhan, P. D. Dernier, and J. P. Remeika, *J. Solid State Chem.* **6**, 419 (1973).
9. M. Marezio and D. P. Dernier, *J. Solid State Chem.* **3**, 340 (1971).
10. H. Horiuchi, M. Tokonami, N. Morimoto, K. Nagasawa, Y. Bando, and T. Takada, *Mater. Res. Bull* **6**, 833 (1971).
11. C. T. Prewitt (unpublished); W. R. Busing, K. O. Martin, and H. A. Levy, ORNL Report No. TM-306 (1964).
12. D. T. Cromer and J. T. Waber, *Acta Cryst.* **18**, 104 (1965); D. T. Cromer, *Acta Cryst.* **18**, 17 (1965).
13. W. R. Busing and H. A. Levy, ORNL Report No. 59-12-3 (1959).
14. J. M. Longo and P. Kierkegaard, *Acta Chem. Scand.* **24**, 420 (1970).
15. L. Pauling, "The Nature of the Chemical Bond," Cornell Univ. Press, Ithaca, NY, 1960.